Fan-shaped Patch Local Binary Patterns for Texture Classification

Yuxing Tang   Charles-Edmond Bichot   Chao Zhu

Université de Lyon, CNRS

Ecole Centrale de Lyon, LIRIS, UMR5205, F-69134, France

{yuxing.tang, charles-edmond.bichot, chao.zhu}@ec-lyon.fr

Abstract

In this paper, we present a new distinctive feature for texture classification, the fan-shaped patch local binary patterns (FP-LBP). The proposed FP-LBP operator extends the traditional LBP operator by encoding the difference between each central pixel with the average value of its neighboring fan-shaped patches, instead of only using its neighboring pixels. By this way, FP-LBP not only preserves more information of local structures than the traditional LBP, but also keeps relatively lower dimensionality, especially when larger radius and more neighboring pixels are considered. Moreover, the "uniform" and rotation invariant FP-LBP are also defined similarly to the traditional LBP. The proposed descriptors are evaluated on two popular texture databases: CUReT and KTH-TIPS, and the experimental results show that FP-LBP outperforms the traditional LBP descriptor with a smaller feature dimension. Moreover, the proposed method achieves higher classification accuracy than most of the state-of-the-art methods on both databases.

1   Introduction

Textures provide significant characteristics for the interpretation and identification of real-world visual patterns. Analysis of texture is important in a wide range of applications and has been an intense research subject in the fields of image processing and pattern recognition. Four major application domains related to texture analysis are texture classification, texture segmentation, texture synthesis, and shape from texture. Among them, texture classification has become a topic of extensive research in the past decades, because of its variety of potential applications such as textile inspection [2], medical imaging [12] and remote sensing [7].

The process of texture classification is often divided into three phases: (1) feature extraction; (2) learning; (3) recognition. In the feature extraction phase, the texture content of all images is captured with the chosen texture analysis approach. The target of the learning phase is to model the texture content of the training images with ground truth labels. In the recognition phase, the texture content of the unknown test sample is represented with the same texture analysis approach, and the test sample is then assigned to the class which has the best match by comparing its texture content with those of the training images by a certain classification mechanism. The major challenge lies in that the real-world textures are usually not uniform due to large variations in illumination, spatial scale, rotation or other visual appearance. Therefore, this paper will focus on the first phase of texture classification by presenting a new texture descriptor.

A large number of texture representations have been proposed in the literature. The representative approaches include: (1) statistical methods, such as generalized co-occurrence matrices [5] and gray level differences [21]; (2) model based methods, such as Markov random fields (MRFs) [1] and fractal analysis [18]; (3) signal processing methods, such as Gabor filtering [11] and wavelet transform [13]. These approaches have been extended later to produce rotation invariant features [17, 19, 15, 20].

Specifically, the local binary pattern (LBP) operator [16, 17] has attracted massive attention because of its discriminative power for texture description and computational efficiency. The original LBP [16] works by comparing the gray value of a central pixel with each value of its 3×3 neighborhood, and by encoding their differences into a binary pattern. The occurrences of the different patterns are then compacted into a histogram as a texture descriptor. The most prominent restriction of the original LBP lies in its small spatial support area, since the features calculated from a local 3×3 window fail to catch large scale structures which might be the determinative information of certain features. Therefore, the LBP operator was later extended to $LBP_{R,P}$ [17], which probes P circularly symmetric neighboring samples on a circle of radius R, instead of a local 3×3 neighborhood. With larger sampling radius and more neighboring samples considered, the operator is able to capture information from a larger spatial area. In addition, op-

erators with varying (R, P) configurations can be brought together to form a multi-scale operator to better describe the texture. Fig. 1 shows three LBP operators with different (R, P) parameters. Although broader range of information can be obtained by considering more neighboring pixels, it also produces feature vectors of higher dimensionality. However, increasing feature vector dimensionality increase the overall computation time more than linearly. For example, $LBP_{4,32}$ and $LBP_{5,40}$ produce histograms of size 2^{32} and 2^{40} respectively, which would be a disaster for computation. To address this problem, Ojala *et al.* improved LBP with "uniform" patterns [17]. Other dimensionality reduction methods for LBP include the center-symmetric local binary patterns (CS-LBP) [10] and the orthogonal combination of local binary patterns (OC-LBP) [23].
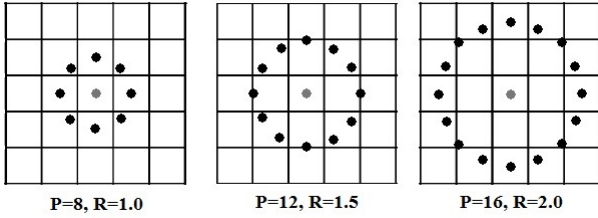

Figure 1. Circularly symmetric neighbor sets for different *(R,P)* **values of LBP.**

Different from the above mentioned approaches, in this paper we propose a new distinctive LBP-based feature, denoted as the fan-shaped patch local binary patterns (FP-LBP), for texture classification. The basic idea of FP-LBP is to extend the traditional LBP operator by encoding the difference between the central pixel value and the average value of the fan-shaped patches of its neighbors, instead of only using its neighboring pixels. The same binary encoding strategy as in LBP is applied to the fan-shaped patches. The proposed FP-LBP operator is able to capture much more significant neighborhood information by considering, for each central pixel's neighbor, larger regions of pixels than LBP. Moreover, for a fixed value of R, dimensionality reduction is achieved by partitioning the neighboring pixels into fewer fan-shaped regions than the usual P number of pixels used for LBP. Similar to LBP, the proposed FP-LBP can also be extended to "uniform" and rotation invariant forms. Multi-scale FP-LBP can be easily realized by concatenating the histograms produced by multiple operators using varying (R, P) parameters.

The rest of the paper is organized as follows. Section 2 reviews the traditional LBP method. In section 3, we present the proposed FP-LBP in detail. In section 4, the proposed feature is experimentally evaluated on two popular texture databases. Section 5 concludes the paper.

2 Brief review of local binary patterns

The local binary pattern (LBP) operator introduced by Ojala *et al.* [17] is a computationally efficient yet powerful means of texture description. It probes an image by comparing, for each pixel of the image, its gray value with each gray value of its neighboring pixels in a sequential, clockwise way. Then, the differences between the central pixel value and its neighboring values are encoded into a binary pattern. Formally,

$$LBP_{R,P} = \sum_{p=0}^{P-1} u(g_p - g_c) \cdot 2^p, u(x) = \begin{cases} 1, & x \geq 0 \\ 0, & x < 0 \end{cases} \quad (1)$$

where g_c is the gray value of the central pixel, g_p is the value of its pth neighbor, P is the total number of neighbors equally located on a circle of radius R. On this circle, if a neighbor position does not perfectly fit with the center of a pixel – as it often occurs, as shown in Fig. 1 – its gray value is calculated by using bi-linear interpolation. The resulting patterns are then accumulated into a histogram to represent statistically the texture content of an image.

The LBP approach has several desirable properties: gray-scale invariance, computational simplicity, and impressive discriminant power. However, the LBP operator produces fairly high dimensional feature vectors (2^P distinct values). This high dimensionality makes it in practice intractable to be used by a classifier for a "large" (> 16) value of P. One solution is to only consider the "uniform" patterns [17]. The U value of LBP is defined as the number of spatial transitions (bitwise 0/1 changes):

$$U(LBP_{R,P}) = |u(g_{P-1} - g_c) - u(g_0 - g_c)| + \sum_{p=1}^{P-1} |u(g_p - g_c) - u(g_{p-1} - g_c)| \quad (2)$$

The patterns which have an U value of at most 2 are defined as "uniform" patterns. Thus, the histogram dimension is reduced to $P(P - 1) + 3$.

Furthermore, the rotation invariant uniform LBP is achieved by the following formulas:

$$LBP_{R,P}^{riu2} = \begin{cases} \sum_{p=0}^{P-1} u(g_p - g_c), & \text{if } U(LBP_{R,P}) \leq 2 \\ P + 1, & \text{otherwise} \end{cases}$$
$$(3)$$

Therefore, mapping from $LBP_{R,P}^{u2}$ to $LBP_{R,P}^{riu2}$ further reduces the length of the feature vector to $P + 2$, leading to a more compact image representation.

3 The fan-shaped patch LBP descriptor

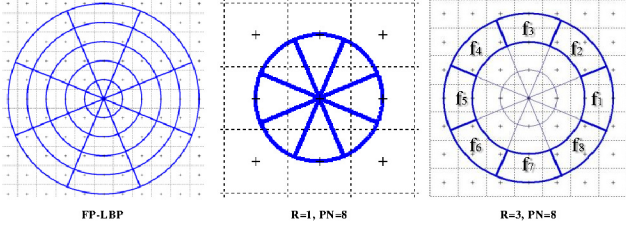As we explained in section 2, the traditional LBP operator, when it considers a large number of neighbors, can

Figure 2. An illustration of the fan-shaped patches in FP-LBP.

Figure 3. An example of the calculation of f_p. Here $f_3 = \frac{\sum_{q=1}^{6}(S_q \cdot g_q)}{\sum_{q=1}^{6} S_q}$.

produce high dimensional histograms which are highly inconvenient to be used by a classifier.

In order to overcome this problem, we propose a new distinctive texture feature, denoted as the fan-shaped (or fan-derived-shaped, hereinafter simply called "fan-shaped") patch local binary pattern (FP-LBP) descriptor.

The basic idea of FP-LBP is that the pixels equidistantly spaced around a circle of radius R in LBP are replaced with equal-area fan-shaped patch regions for encoding, as illustrated in Fig. 2. To encode the fan-shaped patches, the FP-LBP descriptor is defined by comparing the gray value of a given central pixel g_c with the average gray value of its PN neighboring fan-shaped patches $\{f_1, f_2, \ldots, f_{PN}\}$. Following the encoding strategy of LBP, the FP-LBP descriptor is formally defined as:

$$FP - LBP_{R,PN} = \sum_{p=0}^{PN-1} u(f_p - g_c) \cdot 2^p, \qquad (4)$$

where g_c is the gray value of the central pixel ; f_p is the average gray value of its fan-shaped neighborhood ; PN is the total number of the fan-shaped patches located on a circle of radius R ; and $u(\cdot)$ is the function defined in Eq. (1). Particularly, f_p in Eq. (4) can be calculated as:

$$f_p = \frac{\sum_{q=1}^{Q}(S_q \cdot g_q)}{\sum_{q=1}^{Q} S_q} \qquad (5)$$

where each pixel q in an image of size $M \times N$ is assumed to have a square area of size 1×1 ; g_q is the gray value of pixel q ; S_q is the area that pixel q accounts for the total area of the fan-shaped region ; Q is the total number of pixels involved in a particular fan-shaped region. Fig. 3 gives an example of how to calculate f_p.

The resulting binary patterns are then compacted into a histogram as the final FP-LBP descriptor. Compared with the traditional LBP, the proposed FP-LBP considers much more neighboring pixels but produces really lower dimensional feature vectors. Indeed, with FP-LBP, it is no more necessary to have a big value of P when a consistent neighborhood are considered with a large value of R.
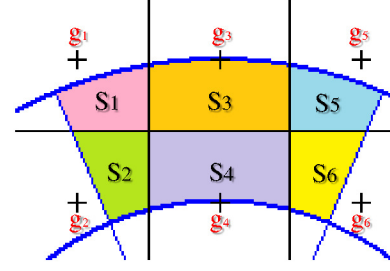
A PN value of 8 is usually large enough. For example, $LBP_{3,24}$ takes 24 neighboring pixels and thus produces a 2^{24} dimensional histogram, while $FP\text{-}LBP_{3,8}$ considers 40 neighboring pixels and only produces a 2^8 dimensional histogram.

Similar to $LBP_{R,P}^{u2}$ and $LBP_{R,P}^{riu2}$, the "uniform" and rotation invariant versions of FP-LBP, respectively denoted as $FP\text{-}LBP_{R,PN}^{u2}$ and $FP\text{-}LBP_{R,PN}^{riu2}$, are also proposed to achieve even smaller feature vector sizes while achieving rotation invariance and keeping good discriminative properties. To attain even larger scale texture structures, we also employ multi-resolution FP-LBP, which can be obtained by concatenating the histograms produced by multiple FP-LBP operators with varying (R, PN) parameters.

4 Experimental evaluation

To evaluate the discriminative power of the proposed FP-LBP descriptor, we conducted a series of texture classification experiments on two popular databases: CUReT [4] and KTH-TIPS [6]. Since the proposed feature is LBP-based, comparisons are first made with the classical LBP schemes presented in [17], including $LBP_{R,P}$, $LBP_{R,P}^{u2}$ and $LBP_{R,P}^{riu2}$/VAR (the joint distribution of $LBP_{R,P}^{riu2}$ and $VAR_{R,P}$ operators). Some comparisons have also been made with other state-of-the-art texture descriptors: CLBP [9], Ex-LBP [14], VZ_MR8 [19] and VZ_Joint [20].

4.1 Experimental setup

Accordingly to section 3, in the following experiments we set the number of patches, PN, as 8 for all the radius R in $FP\text{-}LBP_{R,PN}$.

The proposed FP-LBP descriptor mainly captures local texture information while global texture information is also very important for texture analysis. Thus, in some experiments, we complement the FP-LBP description with global texture information provided by DCI: difference between each central pixel value and the mean value of the whole image. Formally, $DCI = u(g_c - \overline{g})$ where $\overline{g}$ is the average gray value of the whole image and $u(\cdot)$ is the function

Table 1. Classification accuracy (%) of the proposed descriptors compared with LBP on CUReT.

N	46	23	12	6	Bins	46	23	12	6	Bins
(R, P)			(1, 8)					(2, 12)		
$LBP_{R,P}$	89.84	85.03	75.27	65.12	256	91.27	85.99	75.65	66.03	4 096
$LBP_{R,P}^{u2}$	88.95	82.88	72.58	62.82	59	89.71	82.97	74.11	63.72	135
$LBP_{R,P}^{riu2}/VAR$	93.87	88.76	81.59	71.03	160	94.14	89.59	82.17	72.85	224
(R, PN)			(1, 8)					(2, 8)		
$FP\text{-}LBP_{R,PN}$	90.97	84.90	77.60	68.25	256	92.06	86.39	79.60	69.34	256
$FP\text{-}LBP_{R,PN}^{u2}$	90.36	84.51	77.04	67.31	59	90.66	84.60	77.11	67.41	59
$FP\text{-}LBP_{R,PN}/DCI$	94.55	90.18	83.78	74.53	512	95.17	90.71	84.25	74.77	512
$FP\text{-}LBP_{R,PN}^{riu2}/DCI$	91.38	86.63	80.04	70.81	20	88.48	83.50	76.97	67.93	20
(R, P)			(3, 16)					(4, 24)		
$LBP_{R,P}$	93.09	87.24	78.65	68.87	65 536	–	–	–	–	16 777 216
$LBP_{R,P}^{u2}$	91.81	85.95	76.70	68.31	243	93.98	87.85	79.08	69.16	555
$LBP_{R,P}^{riu2}/VAR$	94.20	89.12	81.64	71.81	288	94.84	89.72	81.95	72.14	416
(R, PN)			(3, 8)					(4, 8)		
$FP\text{-}LBP_{R,PN}$	93.77	88.63	81.23	72.03	256	95.11	90.48	83.64	74.52	256
$FP\text{-}LBP_{R,PN}^{u2}$	92.17	86.45	79.20	69.56	59	93.51	88.35	81.62	72.29	59
$FP\text{-}LBP_{R,PN}/DCI$	95.49	91.29	85.24	76.12	512	95.75	91.69	85.65	76.49	512
$FP\text{-}LBP_{R,PN}^{riu2}/DCI$	88.78	83.74	77.24	68.34	20	87.69	81.99	74.84	65.44	20

defined in Eq. (1). The joint descriptor is denoted as FP-LBP/DCI. It can be compared with LBP/VAR [17] which also completes the LBP descriptor with global information.

4.2 Dissimilarity metric and classification principle

After feature extraction, each image in the database is represented as a feature vector. For classification, a classifier associated with certain dissimilarity metric is needed to measure the dissimilarity of the images according to their feature vectors and classify them based on these measurements. As the emphasis of the experiments is to evaluate the discriminative power of the proposed descriptor, a non-parametric classifier is preferred. Here, the chi-square (χ^2) metric as Eq. (6) is utilized to measure the distance between two histograms H and J, and the k nearest neighbor (k-NN) classifier is applied to perform the classification. Specifically, we adopt 1-NN classifier in the following experiments.

$$\chi^2(H, J) = \frac{1}{2} \sum_{i=1}^{K} \frac{(H_i - J_i)^2}{H_i + J_i} \qquad (6)$$

where H_i and J_i are, respectively, the values of the ith bin of the histogram H and J, and K is the length of both histograms.

4.3 Results on the CUReT database

The Columbia-Utrecht Reflectance and Texture (CUReT) database [4] is very challenging for texture classification because of its large intra-class variations and inter-class similarities. It contains images of 61 real-world texture classes (e.g. pebbles, rabbit fur, ribbed paper) photographed under varying illumination and viewing angles. Of the 205 images in each class, 118 images are with the viewing angle less than 60 degree. Following the study of [9], a collection of 92 images are selected from these 118 images for each category. Therefore, the cropped CUReT dataset contains a total number of 5612 (61 × 92) texture images. Varying number of images ($N = 6, 12, 23, 46$) for each category are randomly selected as training set and the rest ($92 - N$) as test set. To avoid bias, 100 random partitions of the dataset are implemented independently. The average classification accuracies over 100 random splits are presented in Table 1.

As shown in the table, $FP\text{-}LBP_{R,PN}$ performs almost always better than $LBP_{R,P}$ while producing a constant vector dimension of 256 where those of $LBP_{R,P}$ dramatically increase. By comparing "uniform" patterns operators, $FP\text{-}LBP_{R,PN}^{u2}$ always outperforms $LBP_{R,P}^{u2}$ while producing even smaller vector dimension. Moreover, it can be noticed that $FP\text{-}LBP_{R,PN}$ steadily performs better than $LBP_{R,P}^{u2}$.

It can also be observed that the joint descriptor $FP\text{-}LBP_{R,PN}^{riu2}/DCI$ achieves lower classification accuracy than $LBP_{R,P}^{riu2}/VAR$, but with a vector dimension 8 to 20 times smaller. Maybe those comparisons are therefore not so relevant. On the other hand, to compare $LBP_{R,P}^{riu2}/VAR$ with a joint FP-LBP/DCI based descriptor of comparable vector dimension, the results of $FP\text{-}LBP_{R,PN}/DCI$ are provided. The latter consistently outperforms $LBP_{R,P}^{riu2}/VAR$. Moreover, FP-LBP/DCI descriptor is training-free, while LBP/VAR needs pre-training to quantize the continuous-valued output produced by VAR. In all the cases above, the proposed descriptors obtain significant improvements compared to the classical LBP

Table 2. Best classification accuracy (%) comparison of the proposed descriptors and other state-of-the-art methods on CUReT.

N	46	23	12	6
$LBP_{R,P}^{riu2}/VAR$[17]	96.04	74.50	–	–
VZ_MR8 [19]	97.43	95.03	90.48	82.90
VZ_Joint [20]	98.03	94.58	89.40	81.06
CLBP [9]	97.39	94.19	88.72	79.98
Ex-LBP [14]	97.29	–	–	–
disCLBP [8]	98.30	96.50	91.90	83.00
$FP\text{-}LBP_{R,PN}/DCI$	97.86	95.31	90.90	85.51

schemes, especially when the number of training samples is relatively insufficient.

Table 2 presents the best classification accuracy of the proposed method and several state-of-the-art approaches on the CUReT database. The best results of FP-LBP/DCI are obtained by using multi-scale $FP\text{-}LBP_{R,PN}/DCI$ with $(R, PN) = (1, 8) + (2, 8) + (3, 8) + (4, 8) + (5, 8)$. Results show that the proposed method outperforms all but one of the state-of-the-art approaches. Indeed, disCLBP [8] always achieves better results but for $N = 6$ where the proposed method is always better.

4.4 Results on the KTH-TIPS database

The KTH-TIPS (Textures under varying Illumination, Pose and Scale) database [6] supplements the CUReT database in a couple of directions, both of which concern extending textual classification algorithms to work in real-world conditions. While the CUReT database contains images of 61 texture classes (over various illumination and pose, but at permanent viewing distance), the objectives of KTH-TIPS are to provide variations in scale, as well as illumination and pose, and to provide images of other samples of a subset of CUReT materials taken under various settings. There are 10 texture classes (e.g. cotton, orange peel, sponge) in KTH-TIPS, each containing 81 images (size 200×200). Hence, the KTH-TIPS dataset contains a total number of 810 (10×81) texture images. Similar to the experimental setup of CUReT, we randomly select 100 different training and test splits, and report the average classification accuracy. The experimental results are presented in Table 3, for training with N images ($N = 5, 10, 20, 40$) and testing with the rest ($81 - N$) per class.

It can be obtained from the table that the mean classification accuracy of $FP\text{-}LBP_{1,8}$ just 0.24% lower than that of $LBP_{1,8}$, but $FP\text{-}LBP_{2,8}$ consistently outperforms $LBP_{2,12}$ by 3.86% higher. Results of $LBP_{3,16}$ and $LBP_{4,24}$ are not provided because of the huge size of their feature vectors. Different from CUReT, the comparisons of "uniform" patterns operators show that $FP\text{-}LBP_{R,PN}^{u2}$

Table 4. Best classification accuracy (%) comparison of the proposed descriptors and other state-of-the-art methods on KTH-TIPS.

M	40	20	10	5
VZ_Joint [22]	92.40	–	–	–
Hayman et al. [22]	94.80	–	–	–
Lazebnik et al.[22]	91.30	–	–	–
Zhang et al.[22]	95.50	–	–	–
Multi-scale BIF [3]	98.50	–	–	–
$FP\text{-}LBP_{R,PN}/DCI$	97.44	92.53	85.03	75.55

is inferior to $LBP_{R,P}^{u2}$, but for $LBP_{1,8}^{u2}$ where $FP\text{-}LBP_{1,8}^{u2}$ performs better.

As for CUReT, the results of $FP\text{-}LBP_{R,PN}^{riu2}/DCI$ are slightly worse than those of $LBP_{R,P}^{riu2}/VAR$, it is probably because of the really tiny size of its vector. However, the results of $FP\text{-}LBP_{R,PN}/DCI$ consistently outperform those of $LBP_{R,P}^{riu2}/VAR$ for comparable vector dimensions.

Table 4 presents the best classification accuracy of the proposed method and several state-of-the-art approaches on the KTH-TIPS database. The best results of FP-LBP/DCI are obtained by using multi-scale $FP\text{-}LBP_{R,PN}/DCI$ with $(R, PN) = (1, 8) + (3, 8) + (5, 8)$. It can be seen that our method outperforms all the state-of-the-art approaches but the multi-scale BIF.

5 Conclusion

This paper presents a distinctive fan-shaped patch local binary pattern (FP-LBP) descriptor for texture classification. The experimental results prove that the proposed feature can effectively describe local texture structures and preserve more significant information than the traditional LBP. Another advantage of the proposed feature is its relatively lower dimensionality, especially when larger radius with more neighboring pixels are taken into consideration. Moreover, the FP-LBP approach is computationally efficient and training-free.

The proposed FP-LBP descriptor is a first study of the use of fan-shaped patch applied to local binary pattern. This work will be extended into several directions including a better representation of neighboring pixels in FP-LBP computation with even smaller feature dimension. It will be also tested on larger scope of applications.

References

[1] R. Chellappa and S. Chatterjee. Classification of textures using gaussian markov random fields. *IEEE Transactions on Acoustics, Speech and Signal Processing*, 33(4):959 – 963, Aug. 1985.

Table 3. Classification accuracy (%) of the proposed descriptors compared with LBP on KTH-TIPS.

N	40	20	10	5	Bins	40	20	10	5	Bins
(R, P)			(1, 8)					(2, 16)		
$LBP_{R,P}$	92.61	86.07	76.85	66.25	256	88.59	81.39	72.65	64.13	65 536
$LBP_{R,P}^{u2}$	90.82	83.05	73.85	64.35	59	91.09	83.80	75.49	65.18	243
$LBP_{R,P}^{riu2}/VAR$	93.38	89.33	82.40	73.57	160	93.85	88.56	81.77	71.85	288
(R, PN)			(1, 8)					(2, 8)		
$FP\text{-}LBP_{R,PN}$	92.35	85.58	76.59	66.31	256	92.74	85.93	76.83	66.68	256
$FP\text{-}LBP_{R,PN}^{u2}$	90.85	83.67	74.65	64.48	59	89.19	81.89	73.07	63.70	59
$FP\text{-}LBP_{R,PN}/DCI$	96.60	91.55	83.75	74.27	512	95.86	90.47	82.66	72.87	512
$FP\text{-}LBP_{R,PN}^{riu2}/DCI$	92.40	87.19	79.83	70.94	20	91.74	85.64	77.86	66.82	20
(R, P)			(3, 24)					(4, 24)		
$LBP_{R,P}$	–	–	–	–	16 777 216	–	–	–	–	16 777 216
$LBP_{R,P}^{u2}$	93.50	86.59	77.05	67.46	555	93.22	85.89	76.17	64.95	555
$LBP_{R,P}^{riu2}/VAR$	92.76	83.83	72.44	62.42	416	92.19	82.74	71.95	61.75	416
(R, PN)			(3, 8)					(4, 8)		
$FP\text{-}LBP_{R,PN}$	93.22	86.15	77.08	66.10	256	93.47	86.75	77.15	65.69	256
$FP\text{-}LBP_{R,PN}^{u2}$	91.37	84.04	75.22	64.99	59	91.88	85.11	75.81	64.90	59
$FP\text{-}LBP_{R,PN}/DCI$	95.70	89.78	81.44	71.56	512	95.40	89.49	80.79	71.00	512
$FP\text{-}LBP_{R,PN}^{riu2}/DCI$	91.64	85.13	76.79	67.43	20	91.18	84.69	76.69	67.40	20

[2] F. Cohen, Z. Fan, and S. Attali. Automated inspection of textile fabrics using textural models. *IEEE Trans. Pattern Anal. Mach. Intell.*, 13(8):803 –808, Aug. 1991.

[3] M. Crosier and L. Griffin. Using basic image features for texture classification. *International Journal of Computer Vision*, 88:447–460, 2010.

[4] K. Dana, B. Van-Ginneken, S. Nayar, and J. Koenderink. Reflectance and Texture of Real World Surfaces. *ACM Transactions on Graphics (TOG)*, 18(1):1–34, Jan. 1999.

[5] L. Davis, S. Johns, and J. Aggarwal. Texture analysis using generalized co-occurrence matrices. *IEEE Trans. Pattern Anal. Mach. Intell.*, 1(3):251 –259, July 1979.

[6] M. Fritz, E. Hayman, B. Caputo, and J.-O. Eklundh. The kth-tips database. http://www.nada.kth.se/cvap/databases/kth-tips.

[7] H. Greenspan and R. Goodman. Remote sensing image analysis via a texture classification neural network. In *Advances in Neural Information Processing Systems 5*, pages 425–432, 1992.

[8] Y. Guo, G. Zhao, and M. Pietikäinen. Discriminative features for texture description. *Pattern Recognition*, 45(10):3834 – 3843, 2012.

[9] Z. Guo, L. Zhang, and D. Zhang. A completed modeling of local binary pattern operator for texture classification. *IEEE Trans. Image Process.*, 19(6):1657 –1663, June 2010.

[10] M. Heikkilä, M. Pietikäinen, and C. Schmid. Description of interest regions with local binary patterns. *Pattern Recognition*, 42(3):425–436, Mar. 2009.

[11] A. Jain and F. Farrokhnia. Unsupervised texture segmentation using gabor filters. *Pattern Recognition*, 24(12):1167–1186, 1991.

[12] Q. Ji, J. Engel, and E. Craine. Texture analysis for classification of cervix lesions. *IEEE Transactions on Medical Imaging*, 19(11):1144–1149, Nov. 2000.

[13] A. Laine and J. Fan. Texture classification by wavelet packet signatures. *IEEE Trans. Pattern Anal. Mach. Intell.*, 15(11):1186 –1191, Nov. 1993.

[14] L. Liu, L. Zhao, Y. Long, G. Kuang, and P. Fieguth. Extended local binary patterns for texture classification. *Image and Vision Computing*, 30(2):86 – 99, 2012.

[15] M. Mellor, B.-W. Hong, and M. Brady. Locally rotation, contrast, and scale invariant descriptors for texture analysis. *IEEE Trans. Pattern Anal. Mach. Intell.*, 30(1):52 –61, Jan. 2008.

[16] T. Ojala, M. Pietikäinen, and D. Harwood. A comparative study of texture measures with classification based on featured distributions. *Pattern Recognition*, 29(1):51–59, Jan. 1996.

[17] T. Ojala, M. Pietikäinen, and T. Mäenpää. Multiresolution gray-scale and rotation invariant texture classification with local binary patterns. *IEEE Trans. Pattern Anal. Mach. Intell.*, 24(7):971 –987, July 2002.

[18] A. Pentland. Fractal-based description of natural scenes. *IEEE Trans. Pattern Anal. Mach. Intell.*, 6(6):661 –674, Nov. 1984.

[19] M. Varma and A. Zisserman. A statistical approach to texture classification from single images. *International Journal of Computer Vision*, 62(1-2):61–81, Apr. 2005.

[20] M. Varma and A. Zisserman. A statistical approach to material classification using image patch exemplars. *IEEE Trans. Pattern Anal. Mach. Intell.*, 31(11):2032–2047, Nov. 2009.

[21] J. Weszka, C. Dyer, and A. Rosenfeld. A comparative study of texture measures for terrain classification. *IEEE Trans. Syst., Man, Cybern.*, 6(4):269 –285, Apr. 1976.

[22] J. Zhang, M. Marszałek, S. Lazebnik, and C. Schmid. Local features and kernels for classification of texture and object categories: a comprehensive study. *International Journal of Computer Vision*, 73(2):213–238, June 2007.

[23] C. Zhu, C.-E. Bichot, and L. Chen. Image region description using orthogonal combination of local binary patterns enhanced with color information. *Pattern Recognition*, 46:1949–1963, July 2013.